The LT1 (paraelectric) phase can be considered as a lock-in of the modulated structure. The presence of twinning domains, with the twin plane (010), is due to two energetically equivalent configurations. The symmetry of this phase is the symmetry of the rotational structure component C_1 and could correspond to a nonpolar soft-mode phase transition.

The incommensurate phase of Cs_2CdBr_4 can be compared with the corresponding modulated phase of K_2SeO_4 (Yamada & Ikeda, 1984) which is stable between 130 and 93 K. In the oxide compound, **q** is approximately twice as large as in the bromide. In addition, the SeO_4 groups have been shown to rotate around **b** (perpendicular to **q**) whereas the $CdBr_4$ groups rotate around **a** (parallel to **q**). In the 'lock-in' phase, K_2SeO_4 is ferroelectric with orthorhombic symmetry while Cs_2CdBr_4 has monoclinic symmetry with a center of inversion. Although the structures are completely isomorphous in the high-temperature phase (same space group and same site symmetries), the comparison indicates the independent evolution of the systems up to the 'lock-in' at low temperature.

The authors would like to thank Dr. A. Yamamoto for his help in the first stages of structure refinement. The crystals were kindly provided by Professor H. Arend. The valuable discussions with B. Doudin are also acknowledged. This work was partially supported by Conselho Nacional de Desenvolvimento Científico e Tecnológico (CNPq-Brazil) and Universidade Federal de Minas Gerais (Brazil).

References

AALST, W. VAN, DEN HOLLANDER, J., PETERSE, W. J. A. M. & DE WOLFF, P. M. (1976). *Acta Cryst.* B**32**, 47–58.
ALTERMATT, D., AREND, H., GRAMLICH, V., NIGGLI, A. & PETTER, W. (1984). *Acta Cryst.* B**40**, 347–350.
AREND, H., MURALT, P., PLESKO, S. & ALTERMATT, D. (1980). *Ferroelectrics*, **24**, 297–303.
BECKER, P. J. & COPPENS, P. (1975). *Acta Cryst.* A**31**, 417–425.
CROMER, D. T. & MANN, J. B. (1968). *Acta Cryst.* A**24**, 321–324.
HEINE, V. & SIMMONS, E. H. (1987). *Acta Cryst.* A**43**, 289–294.
IZUMI, M., AXE, J. D. & SHIRANE, G. (1977). *Phys. Rev. B*, **15**, 4392–4411.
MCCONNELL, J. D. C. & HEINE, V. (1984). *Acta Cryst.* A**40**, 473–482.
MAEDA, M., HONDA, A. & YAMADA, N. (1983). *J. Phys. Soc. Jpn*, **52**, 3219–3224.
PLESKO, S., KIND, R. & AREND, H. (1980). *Phys. Status Solidi A*, **61**, 87–94.
SAWADA, S., SHIROISHI, Y., YAMAMOTO, A., TAKASHIGE, M. & MATSUO, M. (1978). *J. Phys. Soc. Jpn*, **43**, 2099–2102.
STEWART, J. M., KUNDELL, F. A. & BALDWIN, J. C. (1972). The *XRAY*72 system. Tech. Rep. TR-192. Computer Science Center, Univ. of Maryland, College Park, Maryland, USA. Modified by D. SCHWARZENBACH.
WOLFF, P. M. DE, JANSSEN, T. & JANNER, A. (1981). *Acta Cryst.* A**37**, 625–636.
YAMADA, N. & IKEDA, T. (1984). *J. Phys. Soc. Jpn*, **53**, 2555–2564.
YAMAMOTO, A. (1982). *Acta Cryst.* A**38**, 87–92.
YAMAMOTO, A. (1987). Private communication.

Acta Cryst. (1989). B**45**, 26–34

Structural and Thermal Dependence of Normal-Mode Condensations in K_2TeBr_6

BY S. C. ABRAHAMS, J. IHRINGER* AND P. MARSH

AT&T Bell Laboratories, Murray Hill, New Jersey 07974, *USA*

(*Received* 12 *April* 1988; *accepted* 24 *August* 1988)

Abstract

The structural thermal dependence in K_2TeBr_6 resulting from the condensation of normal modes at the monoclinic-to-tetragonal and at the tetragonal-to-cubic phase transitions has been investigated over the temperature range 20 to 430 K. Both single-crystal and powder-profile-fitting structure refinement methods were used, with $\lambda(\text{Mo } K\alpha) = 0.71073$ Å and $\mu = 22.76$ mm^{-1}. $M_r = 685.22$. Phase III is monoclinic, $P2_1/n$, with two K_2TeBr_6 per unit cell and $a^{295\text{ K}} = 7.4908$ (10), $b^{295\text{ K}} = 7.5492$ (7), $c^{295\text{ K}} = 10.6984$ (11) Å, $\beta^{295\text{ K}} = 90.307$ (6)°, $V = 604.98$ (23) Å^3, $D_m = 3.68$, $D_x = 3.761$ g cm^{-3}, $F(000) = 600$; phase II is tetragonal, $P4/mnc$, with two K_2TeBr_6 per unit cell and $a^{410\text{ K}} = 7.5755$ (10), $c^{410\text{ K}} = 10.7702$ (22) Å, $V = 618.1$ (3) Å^3; and phase (I) is cubic, $Fm3m$, with $a^{435\text{ K}} = 10.7456$ (14) Å, $V = 1240.8$ (7) Å^3 and four K_2TeBr_6 per unit cell. In phase III at 295 K $wR = 0.0563$ for 1221 independent averaged $F_m^2 > 4\sigma(F_m^2)$, in phase II at 418 K $wR = 0.0312$ for 302 independent averaged $F_m^2 > \sigma(F_m^2)$ and in phase I at 435 K $wR = 0.0310$ for 58 independent averaged $F_m^2 > \sigma(F_m^2)$. The powder-profile-fitting refinements gave $0.046 \le R_I \le 0.086$ over the entire temperature range. The $TeBr_6^{2-}$ octahedron is very regular, with Te–Br distances of 2.699 (6) Å at 295 K, 2.707 (5) Å at 418 K and 2.695 (3) Å at 453 K after

* Permanent address: Institut für Kristallographie der Universität Tübingen, D7400 Tübingen, Federal Republic of Germany.

0108-7681/89/010026-09$03.00

correction for thermal motion. The atomic coupling between strain tensors and order parameters is treated by group-theoretical normal-mode analysis. The E_g and A_g mode displacements, involving octahedral rotation and cation displacements, are followed in detail between 300 and 434 K. Both monoclinic strain tensors e_{13} and $e_{22}-e_{11}$ become zero simultaneously at 400 K, the tetragonal strain tensor $e_{33}-e_{11}$ becomes zero at 434 K. The transition from phase III to phase II becomes detectable (both from changes in the atomic positions and from the increase in specific heat) slightly above 411 K, a temperature significantly higher than that at which the monoclinic strain tensors become zero.

Introduction

The lattice of a high-symmetry crystal may become distorted by condensation of a normal mode as the temperature is decreased, resulting in lower symmetry below the ensuing structural phase transition. Many cubic crystals undergo a series of such phase transitions on cooling as one or more normal lattice modes successively soften, see Aleksandrov & Misyul' (1981) and Ben Ghozlen & Mlik (1983) for reviews: the latter identify all possible phase symmetries derived from space group $Fm3m$ as prototype. Typical of such high-symmetry crystals are the perovskites (ABO_3 with A usually an alkali or alkaline earth and B a transition tetra- or pentavalent metal atom), the elpasolites ($A_2BB'X_6$, with A an alkali, B a tetravalent, B' a monovalent metal and X a halogen atom), the cryolites (A_3BX_6, with A an alkali, B a trivalent metal and X a halogen atom) and the antifluorites (A_2BX_6, with A an alkali, B a tetravalent and X a halogen atom). Other typical families include the boracites ($A_3B_7O_{13}X$, with A a divalent metal and X a halogen atom), the tungsten bronzes ($AA'_2CBB'_4O_{15}$, with A, A' usually an alkali or alkaline earth, B, B' a tetra- or pentavalent transition metal and C a Li atom, if present) and the langbeinites [$A_2B_2(SO_4)_3$, with A an alkali and B a divalent metal atom], each of which have different prototype space groups.

Within the antifluorite family, K_2TeBr_6 is of particular interest. Three phase transitions have been reported, one between 200 and 240 K (Nakamura, Ito & Kubo, 1962), the others at 405 and 434 K (Rössler & Winter, 1977). The crystal structure of the monoclinic phase at room temperature was initially determined by Brown (1964). Abriel (1983*a*) reported a transition at 445 K from $Fm3m$ to $P4/mnc$ followed by another at 410–334 K to $P2_1/n$, and later gave the corresponding structures at 463 and 423 K (Abriel, 1984). We identified two independent strain-coupled processes that give rise to a broad phase transition centered at about 400 K and found a normal lambda-type phase transition at 434 K in K_2TeBr_6 (Abrahams, Ihringer, Marsh & Nassau, 1984): we also showed that no additional phase transitions took place between 20 and 590 K.

A group-theoretical normal-mode analysis (Ihringer & Abrahams, 1984) showed that both independent modes have E_g symmetry, with one mode producing a displacement of the K^+ ions, the other a rotation of the $TeBr_6^{2-}$ octahedra. The consequent lattice distortion follows a Landau critical power law, with the elastic strain $e_{13} \propto (400-T)^{1/2}$ while $e_{22}-e_{11}=0$ for $T>359$ K. Below 359 K, $e_{22}-e_{11} \propto (359-T)$, but see below for higher resolution results. The coupling between order parameter and elastic strain also gives the cation displacement and anion rotations. A correlation between the change in atomic locations and order parameter as a function of temperature in the phase-transition sequence from $Fm3m$ to $P4/mnc$ to $P2_1/n$ has not previously been investigated and is reported hereunder.

Experimental

Single crystal

Two crystals of K_2TeBr_6, the first with approximate dimensions 0·24 × 0·12 × 0·07 mm,* the second with approximate dimensions 0·11 × 0·30 × 0·38 mm, were selected from a batch grown by the method previously described (Abrahams *et al.*, 1984). D_m was reported previously by Brown (1964). Optical examination of these strong red crystals, which change color to deep red orange (ISCC–NBS, 1964) on extended ambient exposure, revealed no indication of twin components. Each crystal was mounted, in separate experiments, within a microfurnace (Lissalde, Abrahams & Bernstein, 1978) on an Enraf–Nonius CAD-4 diffractometer. Control of measurements on both crystals was by PDP 11/24-8e minicomputer using Enraf–Nonius (1982) software. Mo $K\alpha$ radiation from a graphite monochromator, with ω–2θ scan range of $(0{\cdot}80+0{\cdot}35\tan\theta)°$, was used for the intensity measurements. Backgrounds were estimated by extending the scan 25% on either side of each peak, with maximum time of 240 s spent per reflection for a desired precision in terms of counting statistics of 2%. All reflections within a reciprocal sphere of radius $(\sin\theta)/\lambda \le 0{\cdot}81$ Å^{-1} were measured with $-12 \le h \le 12$, $-12 \le k \le 12$, $-17 \le l \le 17$ at 295 K, $0 \le h \le 12$, $-12 \le k \le 12$, $-17 \le l \le 17$ at 418 K and $-17 \le h \le 17$, $-17 \le k \le 17$, $-17 \le l \le 17$ at 453 K on the first crystal. In addition, all reflections from the second crystal with $-13 \le h \le 13$, $-13 \le k \le 13$, $-19 \le l \le 19$ and $(\sin\theta)/\lambda \le 0{\cdot}90$ Å^{-1} were measured at 295 K.

*This crystal was bounded by tabular $(10\bar{1})$, $(\bar{1}01)$ faces 0·070 mm apart: edge faces, with normal distances to crystal center, were (313), 0·060, $(\bar{3}\bar{1}\bar{3})$, 0·060; (212), 0·065; (010), 0·130; $(\bar{1}\bar{1}\bar{1})$, 0·107; $(1\bar{3}1)$, 0·107 mm. The second crystal exhibited similar morphology.

Lattice constants in the temperature range 20–490 K have been given by Abrahams *et al.* (1984). Absorption corrections, based on the attenuation coefficients in *International Tables for X-ray Crystallography* (1974), were applied in iterative attempts to improve the nominal crystal shape in order to minimize differences among symmetry-equivalent reflections. The resulting maximum, minimum transmission factors for the first crystal were 0·3518, 0·1534 at 295 K; 0·3575, 0·1644 at 418 K; and 0·3892, 0·1823 at 453 K. Corresponding factors for the second and larger crystal at 295 K were 0·148, 0·017. Six standard reflections were measured at intervals of 6 h at each of the three temperatures: temperature stability (K) was $\pm\frac{1}{4}°$, absolute scale $\pm\frac{1}{2}°$. Maximum, minimum intensity variation among the standards was 3·5, 1·5% at 295 K, 7·2, 1·7% at 418 K, and 4·8, 2·3% at 453 K for the first crystal; 8·9, 6·2% at 295 K for the second crystal. The unusually large variation in the standard intensities for both crystals and particularly the second was far from random: distinct steps between nearly invariant long-term plateaus were strongly suggestive of sudden changes in ferroelastic domain orientation. The total number of reflections measured was 10 531 at 295 K, 5788 at 418 K and 1569 at 453 K for the first crystal and 14 957 at 295 K for the second crystal.

Standard deviations (σF_m) of the symmetry-independent averaged structure factors were derived by a variation of Abrahams, Bernstein & Keve's (1971) method in which $\sigma^2(F_m^2)$ is taken as the larger of V_1 or V_2, where V_1 is the internal variance calculated from differences among the members of a form and V_2 is the sum of the variance due to counting statistics and to replication variances in the standards. Reflections with $F_m^2 \leq 4\sigma(F_m^2)$ were omitted from further analysis of the data at 295 K, resulting in 1221 $\langle F_m^2 \rangle$ from the first crystal and 901 from the second. A threshold of $1\sigma(F_m^2)$ used at the higher temperatures resulted in 302 unique reflections at 418 K, and 58 at 453 K, following the averaging of symmetry-equivalent values. $R_{int} = 0{\cdot}0424$ and 0·0466 for the first and second crystals at 295 K with $R_{int} = 0{\cdot}0441$ at 413 K and 0·0408 at 453 K for the first crystal. A normal probability δm plot (Abrahams & Keve, 1971) gave a somewhat nonlinear distribution for each crystal at 295 K, with respective slopes of 0·79 and 1·11. Corresponding plots of the 413 and 453 K δm distribution were also nonlinear to some extent with slopes of 0·89 and 0·68 respectively.*

Brown's (1964) structure at room temperature was confirmed by solving the Patterson function and subsequently using full-matrix least-squares refinement and Fourier series, based on the F_m^2 values from the first crystal. It should be noted that Brown's (1964) atomic coordinates are given in a nonstandard setting, with an acute monoclinic angle and $c > a$ (*cf.* Kennard, Speakman & Donnay, 1967); transformation to an obtuse angle [$\beta = 90{\cdot}307\ (6)°$ at 295 K, see Abrahams *et al.* (1984)], results in a change of sign for his transformed z coordinates. The simplest model in space group $P2_1/n$ at 295 K, in which the atomic coordinates, individual isotropic thermal parameters and scale factor are the only (16) variables, led to $R = 0{\cdot}180$, $wR = 0{\cdot}225$ and $S = 6{\cdot}905$ for the first crystal. All single-crystal least-squares refinements reported herein are based on F_m^2 magnitudes, agreement indicators on F_m magnitudes. The corresponding model with all anisotropic thermal parameters varied (43 total variables) gave $R = 0{\cdot}083$, $wR = 0{\cdot}078$ and $S = 2{\cdot}28$. A significant cause of the poor agreement was anharmonic thermal atomic motion that was particularly notable in the electron density through the Te–Br(2)–Br(3) plane. A fit to the anharmonic motion was hence made by including higher rank tensors, in a Gram–Charlier expansion of the probability density function (Zucker & Schulz, 1982; Johnson, 1969).

The least-squares program of Busing, Martin & Levy (1973) was modified to include higher cumulants and an isotropic extinction correction based upon Becker & Coppen's (1974*a*,*b*) formalism. The best model on the basis of the data from each crystal at 295 K required a fourth-order tensor for the Te atom (all third-order coefficients are necessarily zero at this atomic location; a sixth-order tensor gave further improvement with the first crystal data) and both third- and fourth-order tensors for the Br and K atoms. The final agreement indicators were $R = 0{\cdot}0685$, $wR = 0{\cdot}0563$ and $S = 2{\cdot}19$ for the first (with 187 variables) and $R = 0{\cdot}1011$, $wR = 0{\cdot}0822$ and $S = 1{\cdot}77$ for the second crystal (with 160 variables). The resulting improvement in agreement indicators is highly significant at the 99·5% confidence level for both crystals on including higher cumulants in the refinement model. The relatively poor level of agreement becomes worse as the threshold for including F_m^2 values is decreased, due probably to the presence of twin domains caused by handling the crystal, as indicated by the stepwise variation in standard intensities. Ferroelastic domains, in which atoms with coordinates xyz are transformed to equivalent atoms with coordinates $y\bar{x}z$ as the a and b axes exchange identity, have been observed optically in K_2TeBr_6 crystals, see Abrahams *et al.* (1984). The resulting domain walls may be moved under low applied stress. In addition, twin planes are readily formed as the monoclinic angle β [=90·307 (6)°] is replaced by $180 - \beta$. Scattering from these oriented

* Lists of structure factors (F_m, F_c and σF_m), anisotropic thermal parameters and anharmonic tensor coefficients for the first crystal at 295, 418 and 453 K and for the second crystal at 295 K have been deposited, together with digital values for the powder-profile intensities at eight different temperatures between 20 and 420 K, with the British Library Document Supply Centre as Supplementary Publication No. SUP 51284 (126 pp.). Copies may be obtained through The Executive Secretary, International Union of Crystallography, 5 Abbey Square, Chester CH1 2HU, England.

domains necessarily modifies the values of the measured structure factors.

The final atomic coordinates for both crystals at 295 K are given in Table 1(*a*), transformed to correspond to $c > a$ (as in the *Abstract*) for easier comparison with the structures at higher temperatures. Magnitudes of the anisotropic and anharmonic thermal coefficients have been deposited.* The mosaic radii corresponding to the isotropic extinction parameters are given in Table 1.

The tetragonal structure at 418 K was also solved from the Patterson function and refined by the method of least squares in space group *P4/mnc*. The simplest model with 8 variables, for isotropic temperature factors and neglecting extinction, gave $R = 0{\cdot}199$, $wR = 0{\cdot}139$, $S = 2{\cdot}85$ for 302 $F_m^2 \geq 1\sigma(F_m^2)$. Inclusion of anisotropic thermal parameters in addition to the third- and fourth-rank tensors for the K and Br atoms and fourth-rank tensors only for Te to account for the anharmonic thermal motion, and variation of an isotropic extinction coefficient, gave the atomic coordinates in Table 1(*b*) for a total of 47 variables. The final value of $R = 0{\cdot}0422$, $wR = 0{\cdot}0312$, $S = 0{\cdot}628$. The low minimum observable value of $1\sigma(F_m^2)$ was necessary in view of the number of parameters varied.

The structure of the cubic *Fm3m* phase at 453 K has a single variable position coordinate for Br which is close to $\frac{1}{4}$ in antifluorites. Refinement of an isotropic thermal vibration model, neglecting extinction, gave $R = 0{\cdot}110$, $wR = 0{\cdot}113$, $S = 2{\cdot}160$ for a total of five variables with 58 $F_m^2 \geq 1\sigma F_m^2$. Inclusion of an isotropic extinction correction and anisotropic thermal parameters together with third- and fourth-order tensor coefficients for Br and K and fourth-order coefficients for Te resulted in the coordinates listed in Table 1(*c*) with $R = 0{\cdot}0373$, $wR = 0{\cdot}0310$, $S = 0{\cdot}663$ for the 18 parameters varied.

The final least-squares refinements had maximum values of $\Delta/\sigma = 0{\cdot}05$ at 295 K, 0·03 at 418 K and 0·02 at 453 K. Maximum, minimum features in the final difference electron density map were +2·4, −2·6 at 295 K, +1·3, −0·8 at 418 K and +0·6, −0·1 e Å^{-3} at 453 K.

Powder

Crystals from the same growth batch as that used in the single-crystal studies were ground and sieved to give a particle size less than 50 μm. A layer of K_2TeBr_6 powder 0·1 mm thick was mounted between films of 0·22 mm Kapton in the specimen holder described previously (Ihringer, 1982). The powder diffraction profile was measured at 20 and 300 K in the low-temperature Guinier diffractometer (Ihringer, 1982). A continuous photographic record was also made, using the moving-film adaptation of this instrument with $10 \leq 2\theta \leq 94°$, over the temperature range 20 to 295 K. A high-temperature Guinier diffractometer (Ihringer & Appel, 1984) gave full-profile powder patterns at 330, 354, 375, 396, 411 and 420 K; in addition, a photographic record was again made continuously, as in the low-temperature regime, between 280 and 475 K. Each 180 × 60 mm film was measured, using a slit size of 1·0 × 0·05 mm, in a Joyce–Loebl microdensitometer. Neglecting the edge area, about 150 × 50 mm of film was evaluated, resulting in about 50 profiles per film with 3000 intensity values per profile. Optical density corrections were unnecessary since no film was overexposed. Relative temperature stability was estimated as ±0·1 K below room temperature and ±2 K above. The final temperature scale was obtained by matching lattice constants with the single-crystal data and is estimated as accurate to ±2 K.

Background intensities were determined at 15 to 40 points, calculated either by refining the Gaussian profiles for several reflections (Ihringer & Oswald, 1984) or by inspection in an interactive-graphics mode. In the former, all 50 data sets on a film are determined automatically and checked by linear interpolation between background values for statistical distribution about zero. In the latter, a graphic solution of the Rietveld program (Young, Mackie & von Dreele, 1977) immediately detects any irregularities in background values. Each intensity Y_i on the profiles is given a weight $w_i = [\sigma^2 Y_i + \sigma^2 B_i]^{-1}$, with $\sigma^2 B_i$ for the background B_i taken as constant. The final agreement for all refinements based on film data was rather poor, with $0{\cdot}14 < R_I < 0{\cdot}17$, and this was attributed both to

Table 1. *Atomic coordinates and root-mean-square radial amplitudes of thermal displacement* (Å) *of* K_2TeBr_6

	x	y	z	u_{eq}
(*a*) At 295 K ($P2_1/n$)*				
Te	0	0	0	0·19 (10)
	0	0	0	0·20 (7)
Br(1)	0·0476 (10)	0·0020 (6)	0·2484 (4)	0·28 (12)
	0·0544 (13)	0·0020 (15)	0·2469 (6)	0·26 (9)
Br(2)	0·2842 (8)	−0·2111 (8)	−0·0234 (6)	0·28 (7)
	0·2872 (11)	−0·2145 (18)	−0·0318 (9)	0·24 (10)
Br(3)	0·2087 (8)	0·2872 (8)	−0·0216 (6)	0·28 (5)
	0·2099 (15)	0·2855 (16)	−0·0243 (9)	0·25 (8)
K	−0·0099 (25)	0·4607 (12)	0·2553 (12)	0·33 (14)
	−0·0012 (31)	0·4435 (78)	0·2530 (26)	0·33 (14)
(*b*) At 418 K (*P4/mnc*)				
Te	0	0	0	0·19 (1)
Br(1)	0	0	0·2474 (2)	0·33 (12)
Br(2)	0·2691 (5)	−0·2262 (4)	0	0·32 (10)
K	0	0	0·25	0·34 (4)
(*c*) At 453 K (*Fm3m*)				
Te	0	0	0	0·24 (1)
Br(1)	0·2468 (3)	0	0	0·34 (11)
K	0·25	0·25	0·25	0·33 (1)

* First crystal upper, second crystal lower entry, with coordinates at 295 K transformed to the cell with $a = 7{\cdot}4908$ (10), $b = 7{\cdot}5492$ (7), $c = 10{\cdot}6984$ (11) Å and $\beta = 90{\cdot}307$ (6) Å, see Abrahams *et al.* (1984). The thermal parameter is the r.m.s. radial amplitude. Isotropic extinction mosaic radii are 9·9 (5), 5·4 (4) and 1·0 (5) μm for the first crystal at 295, 418 and 453 K, respectively and 12·3 (1·9) μm for the second crystal at 295 K.

* See deposition footnote.

Table 2. *Atomic coordinates* ($\times 10^4$) *and isotropic thermal parameters* (Å) *by Rietveld analysis refinement of powder diffraction profiles*

		20 K	300 K	330 K	354 K	375 K	396 K	411 K	420 K
Te	u*	0·10 (1)	0·15 (1)	0·16 (1)	0·15 (1)	0·18 (1)	0·13 (1)	0·11 (1)	0·27 (1)
Br(1)	x	725 (6)	578 (6)	546 (7)	524 (8)	457 (9)	335 (15)	245 (25)	0
	y	41 (7)	50 (7)	53 (9)	55 (10)	33 (14)	−30 (23)	−216 (20)	0
	z	2507 (5)	2493 (5)	2484 (6)	2493 (5)	2476 (5)	2459 (5)	2458 (7)	2454 (17)
	u	0·12 (1)	0·22 (1)	0·27 (1)	0·27 (1)	0·29 (1)	0·29 (1)	0·29 (1)	0·19 (1)
Br(2)	x	2956 (7)	2905 (7)	2837 (8)	2841 (9)	2789 (13)	2730 (18)	2709 (24)	2583 (20)
	y	−2014 (8)	−2084 (9)	−2098 (8)	−2098 (9)	−2160 (13)	−2263 (16)	−2300 (17)	−2336 (19)
	z	−390 (5)	−294 (5)	−324 (6)	−276 (7)	−258 (8)	−105 (8)	−72 (12)	0
	u	0·13 (1)	0·22 (1)	0·24 (4)	0·23 (4)	0·25 (4)	0·22 (4)	0·23 (5)	0·42 (1)
Br(3)	x	1991 (7)	2074 (7)	2035 (8)	2061 (9)	2082 (13)	2024 (18)	2021 (23)	2336
	y	2912 (8)	2915 (9)	2885 (8)	2877 (9)	2886 (13)	2984 (20)	2914 (23)	2583
	z	−331 (15)	−244 (5)	−255 (5)	−230 (7)	−198 (8)	−239 (8)	−215 (11)	0
	u	0·14 (1)	0·23 (1)	0·24 (4)	0·23 (4)	0·25 (4)	0·22 (4)	0·23 (5)	0·42
K	x	−240 (14)	−102 (15)	−133 (18)	−106 (21)	−137 (26)	−139 (44)	−249 (64)	0
	y	4345 (11)	4500 (13)	4560 (15)	4617 (18)	4670 (23)	4790 (39)	4895 (31)	$\frac{1}{2}$
	z	2485 (13)	2526 (13)	$\frac{1}{4}$	$\frac{1}{4}$	$\frac{1}{4}$	$\frac{1}{4}$	$\frac{1}{4}$	$\frac{1}{4}$
	u	0·06 (2)	0·22 (1)	0·30 (1)	0·30 (1)	0·31 (1)	0·32 (1)	0·29 (1)	0·45 (1)
R_I		0·075	0·086	0·056	0·052	0·055	0·046	0·048	0·071
R_P		0·17†	0·16†	0·065	0·063	0·067	0·067	0·066	0·14†
R_{wP}		0·19†	0·17†	0·085	0·083	0·090	0·088	0·088	0·19†

* u is the r.m.s. radial amplitude of thermal displacement, with u[Br(2)] set equal to u[Br(3)].
† These indicators were calculated with the background intensities excluded, all others have the background intensities included.

sample preparation and to systematic errors in the gear train of the densitometer. The resulting atomic coordinates, however, clearly indicated that two separate octahedral tilts about the Te–Br(2) and Te–Br(3) axes began at ~420 and ~390 K respectively, both of which increased as the temperature decreased. Below 400 K, the film data showed that K^+ becomes displaced from the $0,\frac{1}{2},\frac{1}{4}$ position along the b direction.

A more definitive determination both of the lattice constants and of the atomic coordinates between 20 and 420 K was derived from the profile refinement of the diffractometer measurements. Full-profile-fitting structure refinement was first undertaken with the 300 K pattern, using the coordinates in Table 1(*a*) as starting model. The final values obtained by least-squares refinement in which $\sum_i[w_i(Y_{m(i)}-Y_{c(i)})^2]$ was minimized ($Y_{m(i)}$ is the ith value of the experimental intensity, $Y_{c(i)}$ the corresponding calculated intensity), were thereupon taken as the starting model for fitting the next adjacent temperature profile. Refinements were made without constraints on the atomic coordinates and with anisotropic temperature factors for all atoms in the monoclinic phase. The imposition of the three constraints for the structure at 420 K: x[Br(2)] = y[Br(3)], y[Br(2)] = $-x$[Br(3)] and z(K) = $\frac{1}{4}$ leads to a smaller R value. The resulting coordinate values are given in Table 2. It may be noted that, although the lattice constants indicate a transition to tetragonal symmetry above 400 K, deviations of the Br(2) and Br(3) z coordinates from zero persist at least to 411 K.

Geometry of $TeBr_6^{2-}$ anion

The atomic coordinates at 295 K given in Tables 1(*a*) and 2 correspond to a very regular $TeBr_6^{2-}$ ion, with Te–Br(1) = 2·680 (4), Te–Br(2) = 2·670 (6), Te–Br(3) = 2·682 (6) Å and all Br–Te–Br angles within 0·6 (2)° of 90° for an average Te–Br distance of 2·677 (6) Å at 295 K for the first crystal; Te–Br(1) = 2·671 (7), Te–Br(2) = 2·713 (10), Te–Br(3) = 2·680 (12) Å and all Br–Te–Br angles within 0·3 (3)° of 90°, for an average Te–Br = 2·688 (22) Å distance for the second crystal at 295 K; and Te–Br(1) = 2·702 (5), Te–Br(2) = 2·704 (5), Te–Br(3) = 2·706 (5) Å and Br–Te–Br angles within 0·3 (3)° of 90°, for an average Te–Br = 2·704 (2) Å for the powder determination at 300 K. Corresponding distances at 418 K, from Table 1(*b*), are Te–Br(1) = 2·663 (4) and Te–Br(2) = 2·665 (3) Å for an average of 2·664 (3) Å. At 453 K the value of Te–Br is 2·652 (3) Å, as obtained from Table 1(*c*). Correction for thermal libration gives an average 2·699 (6) for the first and 2·705 (17) Å for the second crystal at 295 K, 2·707 (5) Å at 418 K and 2·695 (3) Å at 453 K.

Brown (1964) reported an average Te–Br = 2·693 (6) Å distance at room temperature and Abriel (1984) found Te–Br = 2·681 (8) Å at 423 K and 2·676 (2) Å at 463 K in K_2TeBr_6. A simple correction for libration in these two reports gave 2·706 (3) Å at room temperature, 2·720 (5) Å at 423 K and 2·727 (3) Å at 463 K in K_2TeBr_6. Corresponding values in Rb_2TeBr_6 are reported by Abriel & Ihringer (1984) as 2·699 (2) Å in the cubic phase at 160 K and 2·696 (6) Å in the tetragonal phase at 12·5 K. Other recent Te–Br distances reported are 2·753 (2) Å in $[(C_2H_5)_4N]_2TeBr_4.CH_3CN$ by Pohl & Saak (1985), 2·699 (9) Å in *sym*-triphenylcyclopropenylium hexabromotellurate by Borgias, Scarrow, Seidler & Weiner (1985) and 2·699 (13) Å in $[Na(H_2O)_3]_2TeBr_6$ by Abriel (1983*b*).

Neglecting the long Te–Br distance reported in the $TeBr_4^{2-}$ ion and the earlier values reported for K_2TeBr_6, the average of the remaining eight values is 2·700 (4) Å which may be accepted as representative of this distance.

Comparison of multiple K_2TeBr_6 structural determinations

Direct comparison of the three sets of atomic coordinates determined for K_2TeBr_6 at room temperature and the two sets determined both at about 420 and at 455 K may be made by considering determinations in pairs using half-normal probability plots (Abrahams & Keve, 1971). The method depends on plotting the experimental order statistic $\delta p_i = |p(1)_i - p(2)_i|/[\sigma^2 p(1)_i + \sigma^2 p(2)_i]^{1/2}$, where $p(1)_i$, $p(2)_i$ are the ith position coordinates for the first and second experiment and $\sigma^2 p(1)_i$, $\sigma^2 p(2)_i$ are their corresponding variances, against the expected ranked moduli of the normal deviates (as given, for example, in *International Tables for X-ray Crystallography*, 1974).

The experimental order statistics based upon the coordinates derived from the first and second crystals at 295 K as given in Table 1(*a*), and between each of these sets and the coordinates determined at 300 K as given in Table 2, were thereupon plotted against the 12 corresponding ranked moduli of the normal deviates. The only resulting array that was linear, indicating a normal distribution in the order statistics, was for the first crystal taken in conjuction with the powder results. The two other plots had either one (for the second crystal taken with the powder results), or two (for the two single crystals taken together) major inflections in the δp array. It may hence be inferred that the results for the second crystal, the measurement set that is common to both latter arrays, are subject to systematic error. The slope for the linear array is large at about 4·5, and may indicate that the joint standard deviation in atomic coordinates is underestimated by the same factor.

It is noteworthy that, in spite of the statistical evidence for systematic error from different sources being present in each set of measurements, the dimensions of the $TeBr_6^{2-}$ ion remain rather constant for all three sets, see above.

Comparison of the atomic coordinates at 418 K as given in Table 1(*b*) with those reported at 423 K by Abriel (1984) rests upon only three values of δp_i; these are substantially nonlinear, due primarily to the difference in x and y coordinates for Br(2) of nearly 0·10 and 0·07 Å respectively. No conclusions may be drawn for the single atomic coordinate determined at 453 K as given in Table 1(*c*) and that at 463 K as reported by Abriel (1984). However, the differences in Te–Br distance between the pairs of determinations is barely significant, in terms of the stated e.s.d.'s.

Lattice constant and elastic strain critical temperature dependence

The lattice constants of K_2TeBr_6 in monoclinic phase III at 295 K are $a = 7{\cdot}4908$ (10), $b = 7{\cdot}5492$ (7), $c = 10{\cdot}6984$ (11) Å, $\beta = 90{\cdot}307$ (6)° (Abrahams *et al.*, 1984). The a-axis thermal expansion in phase III is described by a polynomial to third order, the b-axis expansion is linear in temperature and the c axis is also described by a polynomial to third order. The monoclinic angle follows a Landau critical power law with $e_{13} \propto (400 - T)^{1/2}$, where the strain tensor $e_{13} = \Delta\beta/2$, see Ihringer & Abrahams (1984). A result of the present series of Rietveld analyses (see Table 2) is the determination of lattice constants with improved precision in the critical temperature interval between 300 and 434 K, as presented in Figs. 1(*a*) and 1(*b*).

The new results completely confirm those given by Abrahams *et al.* (1984) except for that of the b-axis lattice-constant thermal dependence in the important temperature regime between $c/\sqrt{2} \simeq b$ at 275 K and the transition to tetragonal phase II at 400 K. The previous results found $b = 7{\cdot}551$ Å at 298 K and 7·534 Å at 359 K, the temperature at which b appeared to become indistinguishable from a. The assumed

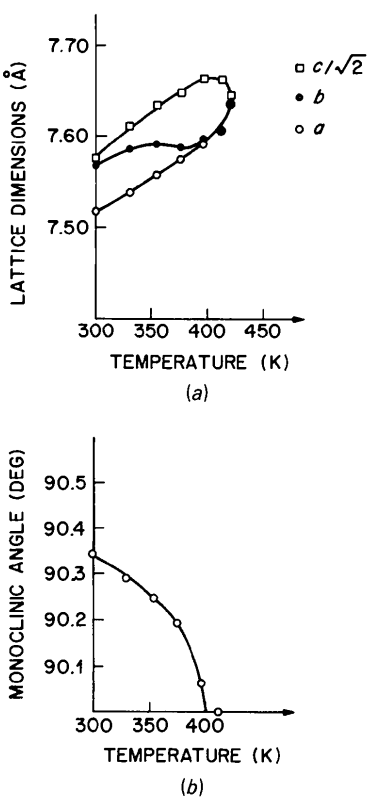

Fig. 1. (*a*) Variation of monoclinic a, b and $c/\sqrt{2}$ lattice constants between 298 and 434 K. (*b*) Variation of monoclinic angle β in same temperature range. One e.s.d. is about 0·001 Å in (*a*) and 0·01° in (*b*).

identity in magnitude of the b and a axes at 359 K indicated that the strain-tensor component $e_{22}-e_{11}$ becomes zero, leading to the possibility that the E_g mode associated with the octahedral order parameter Q^{octa} condenses at this temperature. The present higher resolution results in $b = 7{\cdot}567\,(1)$ Å at 298 K and 7·574 (1) Å at 359 K. Differences between these and the previous measurements are small and without significance. However, examination of Fig. 1(*a*) shows that $b-a = 0{\cdot}030\,(2)$ Å at 359 K and does not become zero until 400 K, the temperature at which $\beta = 90°$ (see Fig. 1*b*) and hence $e_{13} = 0$. It is thus apparent that the order parameters for the E_g mode displacements, with its strong strain coupling involving rotation of the $TeBr_6^{2-}$ octahedra about [010] and displacement of the K^+ ions along [010], reach zero simultaneously at 400 K.

It is also apparent from Fig. 1(*a*) that, in tetragonal phase II between 400 and 420 K, the magnitude of a increases with temperature to coincide smoothly with the decreasing magnitude of $c/\sqrt{2}$ at the transition to the cubic phase, in accordance with the measured heat capacity (Abrahams *et al.*, 1984).

Atomic coupling between strain tensor and order parameter in K_2TeBr_6

The temperature dependence of the atomic coordinates listed in Table 2 is shown graphically in Fig. 2, together with the rotational thermal dependence of Br(2) about Te on the assumption of a rigid $TeBr_6^{2-}$ octahedron. This dependence may be interpreted entirely within the group-theoretical normal-mode analysis of Ihringer & Abrahams (1984). In the phase transition from $Fm3m$ to $P4/mnc$ at 434 K, the tetragonal space group allows opposed octahedral rotations about the fourfold axis [*i.e.* Te–Br(1)], corresponding to A_{2g} symmetry for the soft mode at the X point in the Brillouin zone of the F-centered cubic lattice. The octahedral rotation is the order parameter, which is related to the increasing difference in $c-a$ with decreasing temperature (see Fig. 1*a*) by means of the quadratic expression: $e_{33}-e_{11} = k_A Q_A^2$ (A denotes anion). The effect on the anion rotation is indicated in Fig. 3(*a*).

The expansion in $e_{33}-e_{11}$ between 434 and 411 K is almost linear and obeys the classical Landau relationship $Q_A \propto (T_C - T)^{1/2}$. The octahedral rotation given by A_{2g} symmetry in $Fm3m$ also determines the symmetry

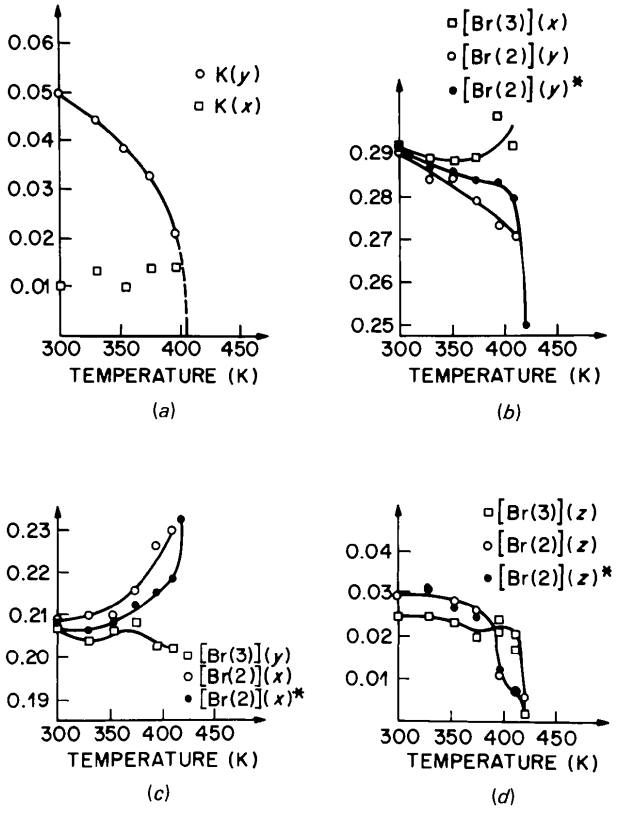

Fig. 2. (*a*) Thermal dependence of K^+ ion x and y coordinates: the z coordinate remains close to $\frac{1}{4}$. (*b*), (*c*), (*d*) Thermal dependence of Br(2) and Br(3) atomic x, y and z coordinates. Br(1) remains close to 0·04, 0·01, $\frac{1}{4}$. Coordinates with asterisks are derived from a rigid $TeBr_6^{2-}$ octahedron. E.s.d.'s are given in Table 2.

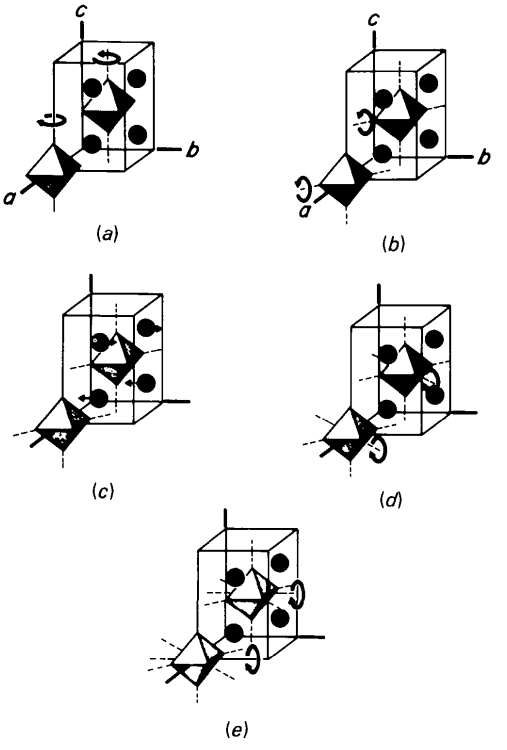

Fig. 3. (*a*) Octahedral rotation in phase transition from $Fm3m$ to $P4/mnc$. In phase transition from $P4/mnc$ to $P2_1/n$: (*b*) Octahedral rotation about Te–Br(2) axis caused by E_g mode. (*c*) Cation displacement caused by E_g mode. (*d*) Octahedral rotation about Te–Br(3) axis caused by E_g mode. (*e*) Octahedral rotation about monoclinic [001], the combination of (*b*) and (*d*).

in the lower temperature phase, *i.e.* $4/mmm$ in space group $P4/mnc$. The rotation in the tetragonal phase is hence of A_{1g} type. Between 420 and 411 K, a gradual transition from $P4/mnc$ to $P2_1/n$ takes place by means of an octahedral tilt about the Te–Br(2) axis, thereby preserving the tetragonal E_g symmetry, as detected in the rate at which the Br(3)z coordinate changes with temperature, see Fig. 2(*d*). The associated order parameter may be designated $Q_E^{\mathrm{Br}(2)}$. The specific heat is also consistent with this interpretation, see Abrahams *et al.* (1984). The small increase in Br(2)z in the same temperature range shows that some E_g-mode symmetry rotation about the Te–Br(3) axis, with order parameter $Q_E^{\mathrm{Br}(3)}$, may also be involved, see Fig. 3(*b*).

Translation by the E_g mode is inconsistent with the A_{1g} octahedral rotation symmetry about the fourfold axis, hence such rotation becomes increasingly inhibited by E_g tilting. The Q_A rotation, which increases 1·64° between ~420 and 411 K, changes only 0·68° between 411 and 396 K. This rotation causes no further increase in $c-a$ through the coupling $e_{33}-e_{11}=k_AQ_A^2$; the corresponding coupling to the octahedral order parameter $Q_E^{\mathrm{Br}(2)}$ is opposite in sign, hence the coupling of $Q_E^{\mathrm{Br}(2)}$ with octahedral rotation is given approximately by $e_{33}-e_{11}=-k_A[Q_E^{\mathrm{Br}(2)}]^2$.

The E_g symmetry displacement of the K^+ ions, primarily along the y direction (see Fig. 2*a*), commences between 411 and 400 K on cooling; the corresponding order parameter may be designated Q_E^{K} (see Fig. 3*c*). The change in monoclinic angle between 411 and 400 K may be described by the linear relationship between strain and order parameter allowed by this symmetry, *i.e.* $e_{13}=k_E^{\mathrm{K}}Q_E^{\mathrm{K}}$. This result is confirmed by a least-squares refinement of the coupling coefficients k_E^{K}, $k_E^{\mathrm{Br}(2)}$ and $k_E^{\mathrm{Br}(3)}$ corresponding to the E_g symmetry order parameters Q_E^{K}, $Q_E^{\mathrm{Br}(2)}$ and $Q_E^{\mathrm{Br}(3)}$, in terms of the change in monoclinic angle as given by e_{13}. Taking $e_{13}=k_E^{\mathrm{K}}Q_E^{\mathrm{K}}+k_E^{\mathrm{Br}(2)}Q_E^{\mathrm{Br}(2)}+k_E^{\mathrm{Br}(3)}Q_E^{\mathrm{Br}(3)}$, the refinement yields $k_E^{\mathrm{K}}=0{\cdot}52\ (6)$, $k_E^{\mathrm{Br}(2)}=0{\cdot}41\ (7)$ and $k_E^{\mathrm{Br}(3)}=-0{\cdot}44\ (12)$, with tilt angles given in radians. The result $k_E^{\mathrm{Br}(2)}\simeq -k_E^{\mathrm{Br}(3)}$ shows that the monoclinic angle is close to being independent of the octahedral rotations provided the rotations about the Te–Br(2) and Te–Br(3) axes are also of comparable magnitude.

It is noteworthy that the phase transition onset from $P4/mnc$ to $P2_1/n$ is most sensitively detected by the change in atomic positions and by the specific heat anomaly, *not* by the change in lattice constants. Deformation of the tetragonal lattice is not very sensitive to the octahedral tilt $Q_E^{\mathrm{Br}(2)}$, although this causes the Br(3)z coordinate to increase sharply from zero between ~420 and 411 K, see Fig. 2(*d*) and also Table 1(*b*).

On cooling, the increasing displacement of the K^+ ions from their tetrahedral interstices located at $0,\frac{1}{2},\frac{1}{4}$ results in contact between nearest K^+ and Br ions in the displacement direction. The octahedron is thereby tilted, for example in the z-axis direction by rotation about the Te–Br(3) axis, as illustrated in Fig. 3(*d*).

Between 396 and 375 K, the E_g symmetry octahedral tilt about the Te–Br(3) axis increases by coupling with the order parameter $Q_E^{\mathrm{Br}(3)}$ very nearly to the angle caused by the $Q_E^{\mathrm{Br}(2)}$ rotation about the Te–Br(2) axis. Both octahedral tilts may be described by a single rotation about $[100]_{\mathrm{mono}}$, see Fig. 3(*e*). This rotation also has E_g symmetry, with order parameter Q_E^{Br} which replaces both $Q_E^{\mathrm{Br}(2)}$ and $Q_E^{\mathrm{Br}(3)}$ in the temperature range over which $Q_E^{\mathrm{Br}(2)}$ and $Q_E^{\mathrm{Br}(3)}$ are equal. Indeed, at the lower boundary of this range, *i.e.* 375 K, the difference between the monoclinic a and b lattice constants becomes unambiguously observable, see Fig. 1(*a*).

Below 375 K, the cation displacement Q_E^{cat} and tilt Q_E^{Br} increase at about the same relative rate on cooling with:

$$[Q_E^{\mathrm{cat}}(20\,\mathrm{K})-Q_E^{\mathrm{cat}}(375\,\mathrm{K})]/Q_E^{\mathrm{cat}}(375\,\mathrm{K})=$$
$$[Q_E^{\mathrm{Br}}(20\,\mathrm{K})-Q_E^{\mathrm{Br}}(375\,\mathrm{K})]/Q_E^{\mathrm{Br}}(375\,\mathrm{K}).$$

It is apparent that these two displacements are linked. Since the cationic displacement gives rise only to the change in monoclinic angle in the present interpretation, it may be assumed that the difference between the a and b lattice constants, which increases almost linearly from 300 to 20 K, is due to the quadratic relationship with order parameter Q_E^{Br}: *i.e.* $e_{22}-e_{11}=k_E^{\mathrm{Br}}(Q_E^{\mathrm{Br}})^2$.

References

ABRAHAMS, S. C., BERNSTEIN, J. L. & KEVE, E. T. (1971). *J. Appl. Cryst.* **4**, 284–290.

ABRAHAMS, S. C., IHRINGER, J., MARSH, P. & NASSAU, K. (1984). *J. Chem. Phys.* **81**, 2082–2087.

ABRAHAMS, S. C. & KEVE, E. T. (1971). *Acta Cryst.* A**27**, 157–165.

ABRIEL, W. (1983*a*). *Mater. Res. Bull.* **18**, 1419–1423.

ABRIEL, W. (1983*b*). *Z. Naturforsch. Teil B*, **38**, 1543–1547.

ABRIEL, W. (1984). *Mater. Res. Bull.* **19**, 313–318.

ABRIEL, W. & IHRINGER, J. (1984). *J. Solid State Chem.* **52**, 274–280.

ALEKSANDROV, K. S. & MISYUL', S. V. (1981). *Sov. Phys. Crystallogr.* **26**, 612–618.

BECKER, P. J. & COPPENS, P. (1974*a*). *Acta Cryst.* A**30**, 129–147.

BECKER, P. J. & COPPENS, P. (1974*b*). *Acta Cryst.* A**30**, 148–153.

BEN GHOZLEN, M. H. & MLIK, Y. (1983). *J. Phys. C*, **16**, 4365–4381.

BORGIAS, B. A., SCARROW, R. C., SEIDLER, M. D. & WEINER, W. P. (1985). *Acta Cryst.* C**41**, 476–479.

BROWN, I. D. (1964). *Can. J. Chem.* **42**, 2758–2767.

BUSING, W. R., MARTIN, K. O. & LEVY, H. A. (1973). *J. Appl. Cryst.* **6**, 309–346.

Enraf–Nonius (1982). *CAD-4 Operations Manual.* Enraf–Nonius, Delft, The Netherlands.

IHRINGER, J. (1982). *J. Appl. Cryst.* **15**, 1–4.

IHRINGER, J. & ABRAHAMS, S. C. (1984). *Phys. Rev.* **30**, 6540–6548.

IHRINGER, J. & APPEL, W. (1984). *Rev. Sci. Instrum.* **55**, 1978–1979.

IHRINGER, J. & OSWALD, M. (1984). Unpublished.

International Tables for X-ray Crystallography (1974). Vol. IV. Kynoch Press. (Present distributors Kluwer Academic Publishers, Dordrecht.)
ISCC–NBS (INTER-SOCIETY COLOR COUNCIL–NATIONAL BUREAU OF STANDARDS) (1964). *Color-Name Charts*, supplement to NBS Circular 553. ISCC–NBS, Washington, DC.
JOHNSON, C. K. (1969). *Acta Cryst.* A**25**, 187–194.
KENNARD, O., SPEAKMAN, J. C. & DONNAY, J. D. H. (1967). *Acta Cryst.* **22**, 445–449.
LISSALDE, F., ABRAHAMS, S. C. & BERNSTEIN, J. L. (1978). *J. Appl. Cryst.* **11**, 31–34.
NAKAMURA, D., ITO, K. & KUBO, M. (1962). *J. Am. Chem. Soc.* **84**, 163–166.
POHL, S. & SAAK, W. (1985). *Z. Naturforsch. Teil B*, **40**, 251–257.
RÖSSLER, K. & WINTER, J. (1977). *Chem. Phys. Lett.* **46**, 566–570.
YOUNG, R. A., MACKIE, P. E. & VON DREELE, R. B. (1977). *J. Appl. Cryst.* **10**, 262–269.
ZUCKER, U. H. & SCHULZ, H. (1982). *Acta Cryst.* A**82**, 563–568.

Acta Cryst. (1989). B**45**, 34–40

Atomic Displacement, Anharmonic Thermal Vibration, Expansivity and Pyroelectric Coefficient Thermal Dependences in ZnO*

J. ALBERTSSON† AND S. C. ABRAHAMS
AT&T Bell Laboratories, Murray Hill, NJ 07974, *USA*
AND Å. KVICK
Chemistry Department, Brookhaven National Laboratory, Upton, NY 11973, *USA*

(*Received* 25 *April* 1988; *accepted* 11 *August* 1988)

Abstract

The thermal expansivity in zinc oxide, space group $P6_3mc$, has been remeasured dilatometrically in the range 298–900 K and normalized to the lattice constants measured at 298 K in a Bond lattice-constant diffractometer. The lattice constants have also been determined at 20 K in a four-circle diffractometer. The linear thermal-expansion coefficients are $\alpha_1^T = 6{\cdot}511 \times 10^{-6}[1 + 0{\cdot}693\,(20) \times 10^{-3}\Delta T - 0{\cdot}230\,(6) \times 10^{-6}(\Delta T)^2]\ K^{-1}$ and $\alpha_3^T = 3{\cdot}017 \times 10^{-6}[1 + 2{\cdot}56\,(7) \times 10^{-3}\Delta T - 3{\cdot}37\,(9) \times 10^{-6}(\Delta T)^2]\ K^{-1}$, where $\Delta T = T - 298$ K. The structure has been determined at 20, 300, 600 and 900 K by neutron diffraction, based respectively upon 584, 301, 364 and 364 symmetry independent averaged F_m^2. Evidence for thermal atomic vibration anharmonicity was present at 600 and 900 K, but was not detectable at 20 and 300 K. Appreciable extinction was found at all temperatures. The ionic displacement thermal-dependence coefficient is $0{\cdot}263\,(8) \times 10^{-4}$ Å K^{-1} between 20 and 900 K. The pyroelectric coefficients derived from a point-charge model, with point charge of $0{\cdot}21\,(5)e$ and nuclear positions corresponding to final $R = 0{\cdot}0225$, 0·0231, 0·0177 and 0·0182 at 20, 300, 600 and 900 K respectively, are +1(2), −11(4) and −11(5) × 10^{-6} C m^{-2} K^{-1} at 160, 450 and 750 K respectively compared with experimental values of −6, −10·3 and $-11{\cdot}6 \times 10^{-6}$ C m^{-2} K^{-1}.

* Part of this work was performed at the Brookhaven National Laboratory under contract DE-AC02-76CH00016 with the US Department of Energy and supported by its Division of Chemical Sciences, Office of Basic Energy Sciences. The work was also supported in part by the Swedish Natural Science Council.

† Permanent address: Inorganic Chemistry 2, Chemical Center, University of Lund, POB 124, S-22100 Lund, Sweden.

0108-7681/89/010034-07$03.00

Introduction

The microscopic origin of pyroelectricity in polar crystals has long been a topic of considerable interest. A direct relationship between atomic displacement and polarization temperature dependence has been developed in recent years for several pyroelectric crystals, see reviews by Abrahams (1978, 1979, 1985). Typical values of the pyroelectric coefficient range from 300 × 10^{-6} C m^{-2} K^{-1} for $BaMnF_4$ to $-3{\cdot}9 \times 10^{-6}$ C m^{-2} K^{-1} for $LiClO_4.3H_2O$, with larger values being generally associated with ferroelectric crystals. These coefficients have been used to derive the corresponding ionic displacement temperature coefficients; that for $BaMnF_4$ is $0{\cdot}9 \times 10^{-3}$ Å K^{-1} and for $LiClO_4.3H_2O$ is $0{\cdot}03 \times 10^{-3}$ Å K^{-1}, for example. Among the first pyroelectric crystals for which the ionic displacement temperature coefficient was measured experimentally in relation to the pyroelectric coefficient was $Ba(NO_2)_2.H_2O$ (Liminga, Abrahams, Glass & Kvick, 1982); with a value for the compound of $0{\cdot}44\,(1) \times 10^{-3}$ Å K^{-1}, a polarization change of $-3{\cdot}0 \times 10^{-3}$ C m^{-2} was calculated between 102 and 298 K compared with a measured value of $-2{\cdot}6 \times 10^{-3}$ C m^{-2}. Similarly, the polarization change in $Li_2SO_4.H_2O$ between 80 and 298 K was calculated from the nuclear positions as $-11{\cdot}8 \times 10^{-3}$ C m^{-2} (Karppinen, Liminga, Kvick & Abrahams, 1988),